

Robust μ -synthesis Loop Shaping for Altitude Flight Dynamics of a Flying-Wing Airframe

Fendy Santoso^{1,3}, Ming Liu^{2,3}, Gregory K. Egan³

¹Graduate School of Biomedical Engineering
The University of New South Wales, Australia

²Institute of Intelligent Machines
Chinese Academy of Sciences, Hefei, China

³Department of Electrical and Computer Systems Engineering
Monash University, Australia

Email: fendy.santoso@unsw.edu.au

Abstract

In this paper we present a centralised flight-by-wire system based on μ -synthesis approach to the longitudinal flight motion of our experimental flying wing unmanned aerial vehicle (UAV), P15035 series. The challenge associated with our UAV is related to the fact that all motions of our UAV are controlled by two independently-actuated-ailerons namely elevons, together with its throttle. The scope of this research, nonetheless, falls within the area of elevon control based on the trimmed linear longitudinal flight modes obtained experimentally while throttle was set constant. The reason for considering μ -synthesis autopilot is to minimise the effects of uncertainty in modelling by maximising the amount of tolerable uncertainty within our system's bandwidth as we aim to minimise the structure singular value μ of the corresponding robust performance associated with the uncertain systems. Second, it also provides flexibility in tuning due to the absence of partitioning model of MIMO system. Hence the entire autopilot was designed by keeping the system model as a whole. We also perform a comparative study with respect to well-known H_∞ mixed sensitivity autopilot. Our study indicates that the μ synthesis autopilot designed possesses better performances both in time and frequency domain as indicated by reasonably quick settling time in the absence of overshoot while still maintaining better robust stability margin.

Index Terms: Robust μ -synthesis Autopilot, Uncertainty, Flying-Wing UAV

I. Introduction

A

Autonomous flying robots, which is also colloquially known as Unmanned Aerial Vehicles (UAVs) or “drones” have been widely developed for purposeful civilian and military applications such as aerial surveillance, inspection in complex and inhospitable environments, agriculture, mapping and analysis, animal tracking, border protection, wildlife habitat monitoring, missions in hostile environments, volcano observations *etc* [1-5]. One major challenge on the designs of UAVs is due to development of robust autopilot systems that can provide autonomous guidance from taking-off, cruising to landing in the face of uncertainty and modelling errors. The reason is because there is no perfect mathematical model for any systems in the world, even for the very basic and simplest one.

As such, every mathematical model, regardless its complexity is subject to modelling error. For this reason, therefore, we must be aware of the issue of modelling error and its propagation with respect to the performance of the overall closed-loop control systems.

Furthermore, given the fact that the identified models will be used to design the real-time control systems, improper handling of uncertainty shall adversely affect the robustness of the closed loop control systems. In worst case, the proposed systems may not work practically due to lack of robustness.

Accordingly, robust control systems have been widely developed [6-16]. To name a few, while Balas *et al.* discussed the application of μ -synthesis techniques to momentum management and attitude control of the space station [6] and the same author in [7] also developed robust control of flexible modes in the controller crossover region, Doyle *et al.* in [8] formulated state-space solutions to standard H_2 and H_∞ control problems. Furthermore, while a case study of space shuttle lateral axis flight control system during re-entry was thoroughly discussed in [11], linear-multivariable robust control with a μ perspective was proposed in [10] by Packard *et al.*.

Considering autonomous flight control systems, the ultimate design that the UAV engineers wish to achieve is to provide autonomous guidance from taking-off, cruising to landing. In order to achieve this goal, feedback control systems must satisfy both robust stability and robust performance for a particular dynamic system.

Accordingly, our motivations to conduct this research are threefold and they can be elaborated as follows. First, the reason to employ μ -synthesis robust autopilot is to design a robust compensator in frequency domain in a way that we can maximise the robust stability margin of the closed-loop control system with respect to modelling error within the operational bandwidth of the system.

To address this question, we employ a centralised robust autopilot that is easy to tune by means of unpartitioning system’s model while considering the dynamics of sensor noise, external disturbance (*e.g.* wind gust) and error in modelling. Second, we also aim to achieve a responsive time domain closed-loop response with minimum overshoot. This is critical since the presence of overshoot is undesirable, a waste of energy and it can cause serious damage on the aircraft, particularly when the aircraft is about to land.

Hence, our main goal is to minimise the structure singular value μ of the corresponding robust performance associated with the uncertain system. We believe that this method is more powerful and easier to be computed and implemented compared to conventional robust control approaches (*e.g.* H_∞ or H_2 counterparts). Subsequently, we also perform a comparative study to compare the performance of our μ -synthesis autopilot with respect to H_∞ counterpart.

In more detail, we consider designing μ -synthesis autopilot via D-K iteration. The D-K iteration procedure is an approximation to μ -synthesis control design. The availability of μ -synthesis toolbox in MatLab® has simplified the composition process. The offline computation algorithms also have made the composition process more computationally intensive rather than the real time control loops computed in flight, where we have electrical and computational power limitations.

Our research aircraft P15035 (see Fig. 1) belongs to the class of aircraft called flying wings and is known colloquially as a ‘plank’ having an unswept constant chord (width) wing of low aspect (length-to-width) ratio and no rudder or elevator in the sense of a more conventional aircraft.

We chose a plank since it is very rugged, of compact construction and has, at least for human pilots, very benign flight behaviour and wide airspeed range; autopilot design and tuning is a little more challenging compared to conventional aircraft.

Meanwhile, our technical reason for considering a flying wing aircraft is due to its unique advantage compared to conventional aircraft that normally has three control surfaces. The benefit is due to reduced parasitic drag in the absence of an extended tail and associated elevator and rudder control surfaces. Subsequently, this leads to the second motivation of this research to substantiate the mathematical model of the longitudinal dynamic behaviours of a typical flying wing UAV.

This type of aircraft is well-known and has been widely developed, especially for purposeful military applications such as in “stealth technology” which is a low-observable-type aircraft designed to avoid radar detection using various state-of-the-art counter-detection technologies that reduce the reflection of radar, infra-red, visible light as well as RF spectrum. Hence, the aircraft can camouflage and remains undetected by various electromagnetic spectrums.

Some examples of typical real flying wing type aircraft in military domain are due to B2-strategic bomber, Northrop YB-49 as well as Lockheed Martin RQ-170 Sentinel UAV employed by United States Air Force. Hence, this study can also serve as comparative investigation of the dynamic behaviors of typical flying wing aircraft and its possible extension or modification such as bi-directional flying wing developed by NASA for supersonic travel.

Technically, our P15035 has two elevon control surfaces which combine the functions of elevators and ailerons in which its technical specification are illustrated on Table 1. While pitch is controlled by

the average deflection of the elevons, roll is by the difference. Furthermore, while the aircraft has a vertical stabiliser, it has no attached rudder and so yaw control is indirect through roll.

The aircraft does not have the usually long moment arm provided by elevators, it must rely upon a trailing edge reflex in the rear of the airfoil to maintain a positive pitching moment to overcome the moments introduced by a forward centre of gravity this being essential to maintain stability. Partially as a consequence of this, there is an increased coupling between throttle and pitch. We have assumed constant cruise throttle setting in this paper.

TABLE I: SPECIFICATIONS OF AIRCRAFT P15035

Span	150 cm	Motor	Electric
Chord	35 cm	Duration	40-60 minutes
Length	106 cm	Speed	33 to 150 Kph
Control Surface	Elevon	Battery	28×GP3300NiMh
Weight	2.9-4.6 kg	Autopilot	MP2028

In addition, for the purpose of performing experimental-based modelling, we have at our disposal a large repository of flight logs for our aircraft. It contains the complete dynamics record of flight data.

To further complicate matters, we fly at relatively **at** low Reynolds number (<250K) regimes, which means turbulent flow and laminar separation occurs across wing surface. Air turbulence is also of concern due to the size of the aircraft; see [17] for more comprehensive explanations. As a result, the aircraft dynamics are non-linear and at times varying. Interested readers are suggested to refer to [17-19]. More comprehensive information regarding this small UAV controls will be given in Section II.



Fig. 1 The P15035 Aircraft (Reproduced with the permission of J. Bird, a then member of the then Monash Aerobotics® Research Group)

Given the non-linear inherit behaviours of aircraft dynamics, it is worth considering to employ non-linear modeling and autopilots *e.g.* while Melin in [20] considered Neuro-Fuzzy fractal approach for adaptive-based control of an aircraft, Ye in [21] investigated equational dynamic modelling and adaptive control for a UAV. Moreover, Escareño in [22] studied non-linear modelling and control of a convertible VTOL aircraft in hover mode, Rimal et al. in [23] conducted simulation of non-linear identification and control of a UAV by means of artificial network. Furthermore, George et al. in [24] developed a Simulink model for an Aircraft landing system using energy functions.

In this work, however, we develop linear robust autopilot via μ -synthesis due to its simplicity, practicality as well as robustness as earlier studied in [25] and [26]. Our preliminary work on optimal and robust autopilot can be found in [27-29]. Relevant control theory related to system identification can be found in [30-35].

The organisation of this paper is as follows. Firstly, Section I depicts the motivations and the organisation of this research. In Section II, the open loop mathematical model of elevon-average-to-altitude is introduced together with the study of its time domain characteristics. Next, Section III deals with robustness issues. Subsequently, in section IV robust autopilot via μ -synthesis has been introduced together with the study of both their frequency domain as well as time domain performances. Lastly, conclusions will be drawn in Section V.

II. Open Loop Elevon-Average-to-Altitude Mathematical Model

Longitudinal and lateral models for conventional larger aircraft are well understood; see [26-28]. It is assumed that the longitudinal dynamics is to be uncoupled from its lateral motions. Pitch is controlled by the average deflection of the elevons, meanwhile, roll is controlled by the elevon deflections in an attempt to control yaw and to minimise the adverse drag.

The longitudinal directional models for the P15035 were obtained using system identification techniques. Consider the trimmed model in which the throttle is constant, two controllable inputs of the model are right elevon, left elevon and three outputs are given by output state vector $[q, p, r]^T$, representing the rates of pitch, roll and yaw vectors, respectively. Hence, the linear trimmed model of our flying wing UAV can be depicted as follows [17]:

$$\begin{bmatrix} p \\ q \\ r \end{bmatrix} = \begin{bmatrix} G_{11} & G_{12} \\ G_{21} & G_{22} \\ G_{31} & G_{32} \end{bmatrix} \begin{bmatrix} \delta_l \\ \delta_r \end{bmatrix}, \quad (1)$$

where δ_l, δ_r represent left and right elevon respectively (degree) and G_{ij} are the corresponding transfer functions.

Due to the symmetrical properties of the aircraft about its x - z plane, consequently, the effects of left and right elevons are identical to the pitch but opposite to the roll and yaw, therefore we have that $G_{11} = G_{12}$, $G_{21} = -G_{22}$, $G_{31} = -G_{32}$. By denoting $G_P = G_{11}$, $G_R = G_{21}$ and $G_Y = G_{31}$, it eventually leads to the following equation [12], [13]:

$$\begin{bmatrix} p \\ q \\ r \end{bmatrix} = \begin{bmatrix} G_P & 0 \\ 0 & G_R \\ 0 & G_Y \end{bmatrix} \begin{bmatrix} \delta_A \\ \delta_D \end{bmatrix}, \quad (2)$$

where, respectively, δ_A and δ_D are associated with elevon average and elevon difference, given by $\delta_A = \delta_l + \delta_r$ (or $\delta_A = (\delta_l + \delta_r)/2$), if G_P becomes $2G_P$) and $\delta_D = \delta_l - \delta_r$. From equation (2), pitch is independently controlled by elevon average deflection δ_A , corresponding to the elevators of a conventional aircraft; and roll and yaw are both driven by elevon difference δ_D , corresponding to the aileron and rudder for a conventional aircraft. Consequently, no decoupling can be made between yaw and roll due to special configuration of the aircraft.

The control schemes generally on our UAV have a classic inner and outer loop configuration. The selection of 5Hz was determined by the manufacturers of the autopilot since we use Micropilot MP2028.

2.1 Pitch Rate-to-Pitch Modelling

The input-output experimental data of pitch-rate-to-pitch is represented in Fig 2.

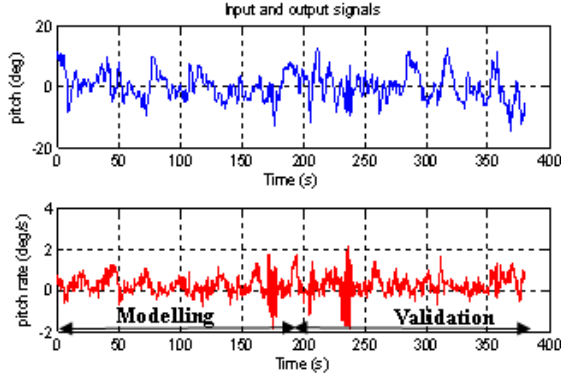


Fig. 2 Flight Logs of Pitch-Rate-to-Pitch Transfer Function

Accordingly, the relation of pitch-rate-to-pitch can be obtained as follows:

$$\left. \frac{\theta_p}{p} \right|_{5\text{Hz}} = \frac{0.2009z}{z-0.9785} \text{ (deg/s)} = \frac{0.00349z}{z-0.9785} \text{ (rad/s)}$$

The model can be validated as seen in Fig. 3 as follows:

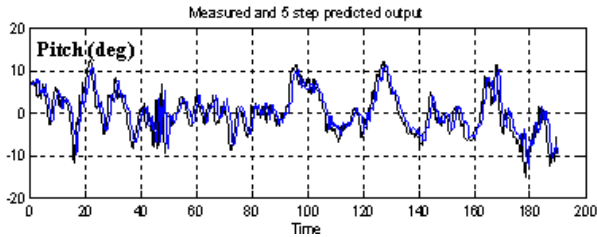


Fig. 3 Measured (black line) and Simulated (blue line) Pitch (in degree)

Since the difference between the measured data and simulated model is negligible, it can be argued that the acquired model is valid.

By cascading the relation of elevon-average-to-pitch-rate as well as pitch-rate-to-pitch, under trimmed flight conditions with a constant engine throttle and airspeed, the P15035's longitudinal

discrete time transfer function from the elevon average deflection δ_a in degree to the pitch angle θ_p ($^\circ$) with a sampling frequency of 5 Hz is $\left. \frac{\theta(z)}{\delta(z)} \right|_{5\text{Hz}} = \frac{-0.1306z^2(z+0.009)}{(z-0.9115)(z-0.9785)(z^2+0.226z+0.376)}$, (3) in which its complex conjugate poles are given by: $z = -0.1134 \pm 0.6029i$.

Converted (3) to s domain model, using zero order hold on the inputs it becomes: (4)

$$\frac{\theta(s)}{\delta_a(s)} = \frac{-0.2954(s+6.693)(s^2+11.7s+91.49)}{(s+0.4633)(s+0.1087)(s^2+4.887s+83.12)}$$

, with a pair of complex conjugate pole given by: $s = -2.4435 \pm 8.7835i$.

It is well known; e.g. see [19], [20] that the typical longitudinal dynamics of a conventional aircraft (elevator to pitch) with a constant engine throttle can be mathematically expressed as follows:

$$\frac{\theta(s)}{\delta(s)} = \frac{k_\theta (s+1/T_{\theta_1})(s+1/T_{\theta_2})}{(s^2+2\zeta_p\omega_p s+\omega_p^2)(s^2+2\zeta_s\omega_s s+\omega_s^2)}. \quad (5)$$

In (5) δ is now the elevator angle (instead of the elevon average in (4)); k_θ is the high frequency gain; $\Delta s_p = s^2 + 2\zeta_p\omega_p s + \omega_p^2$ is the so-called phugoid mode, and $\Delta s_s = s^2 + 2\zeta_s\omega_s s + \omega_s^2$ is the short period mode; ζ_p and ζ_s are the damping factors and ω_p and ω_s are the undamped natural frequency of the two modes, respectively.

Typically, the phugoid mode is overdamped with a relatively large time constant and the short period mode represents underdamped oscillations. The overall pitch step response is a combination of a slow exponential function and quickly decaying high frequency oscillations.

Also, comparing (4) with (5), it can be apparently seen that the longitudinal model (4) has pitch characteristics which are not exactly the same as those of conventional aircraft. Consequently, when the roots are real, the term phugoid can no longer be properly used.

In this regards, its phugoid model is replaced by pitch subsidence roots and is given by: $\Delta s_p = (s + 0.4633)(s + 0.1087)$

This is overdamped with a dominant large time constant of $\tau = 10s$. Its short period model is given by:

$$\Delta s_s = s^2 + 4.887s + 83.12 \quad (5)$$

Here, the damping ratio is about 0.268 and the natural frequency 9.12 rad/s. The settling time is small being in the order of 1s. The impulse response for both modes is plotted in Fig. 4. Normally, the roots of the phugoid mode are complex conjugate.

In more detail, a comparative computer simulation of impulse pitch amplitude response for short term and subsidence mode can be seen in Fig. 4. It is apparent that the short period mode response dies much quicker, in the order of 25 times faster than the impulse response from subsidence mode.

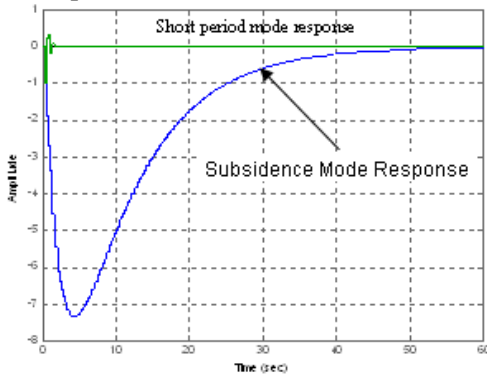


Fig. 4 Impulse pitch amplitude responses (deg) for phugoid and short period modes of UAV P15035

Fig 4 also turns out that the final dc values of both pitch and altitude with respect to a unit step input are negative constants with different nominal values *i.e.* $-k$ and $-c$, where $k \neq c$, as expected in real flight.

2.2 Pitch-to-Altitude Modelling

Pitch-to-altitude transfer function can be modelled using a block diagram given in Figure 5.

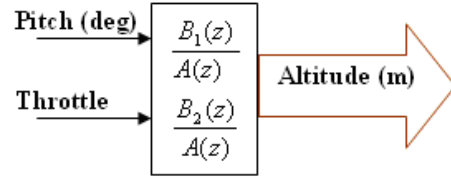


Fig. 5 Relation of Pitch-and-Throttle-to-Altitude

Pitch and throttle are in fact two major inputs to altitude control, hence, this system can be modelled using two transfer functions, *i.e.*, $B_1(z)/A(z)$ represents the dynamics of pitch-to-altitude and $B_2(z)/A(z)$ depicts the dynamics of throttle-to-altitude.

However, since it is assumed that the engine should produce a constant throttle, the influence of $B_2(z)/A(z)$ can be neglected. Hence, for modelling, the first 950 data points were examined, whilst data number 951-1800 were used for validation. Again, this also happens under an assumption that the aircraft experienced small or negligible perturbation during its period of flight.

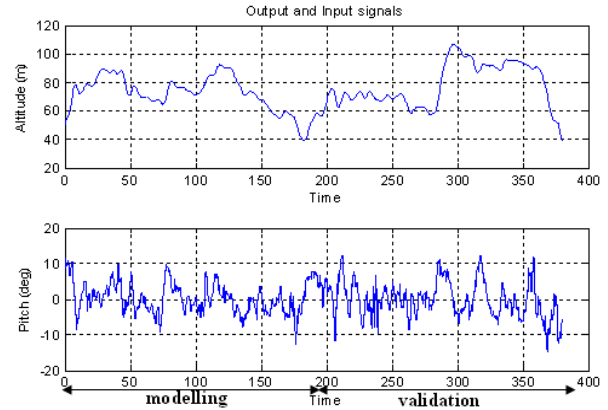


Fig. 6 Pitch-to-Altitude Experimental Data

As can be seen in Fig. 6, the input variable is the pitch angle in degrees. It was perturbed in small angles around $-\pi/18$ to $\pi/18$ in order to achieve its desired altitude. Also, it should be pointed out that the open loop data was obtained during real-time flight test using an experienced human pilot mode to really achieve reasonably accurate experimental data.

The resulting discrete transfer function of pitch-to-altitude is obtained as:

$$\left. \frac{h(m)}{\theta_p(\text{deg})} \right|_{5\text{Hz}} = \frac{0.05456z}{z-0.9969} \quad (6)$$

Furthermore, by cascading the relation of elevon-average-to-pitch; i.e. with pitch-rate-to-pitch as well as pitch-to-altitude, hence, the resulting transfer function of the overall longitudinal motion is obtained as: (7)

$$\left. \frac{h}{\delta_a} \right|_{5\text{Hz}} = \frac{-0.007128z^3(z+0.0091)}{(z-0.9115)(z-0.9785)(z-0.9969)(z^2+0.2267z+0.3763)}$$

From (7) the linearised model of the longitudinal dynamics can be expressed in continuous state space equations given by:

$$\begin{aligned} \dot{x} &= Ax + Bu \\ y &= Cx + Du \end{aligned} \quad (8)$$

in which, $u = \delta_a$, $y = h$ and x is the state vectors of the systems depicting altitude, pitch, pitch rate as well as second and third derivatives of pitch while A and B denote systems' matrices and C as well as D indicate outputs of the system.

$$A = \begin{bmatrix} -5.4740 & -86.0500 & -49.120 & -4.9270 & -0.0650 \\ 1 & 0 & 0 & 0 & 0 \\ 0 & 1 & 0 & 0 & 0 \\ 0 & 0 & 1 & 0 & 0 \\ 0 & 0 & 0 & 1 & 0 \end{bmatrix},$$

$$B = [1 \ 0 \ 0 \ 0 \ 0]^T,$$

$$C = [-0.0117 \ -0.2519 \ -3.0060 \ -18.640 \ -49.4200], \quad D = [0],$$

where x_5 is altitude of the aircraft (m), x_4 is pitch output (deg) and x_3 to x_1 are the first to third derivative of pitch.

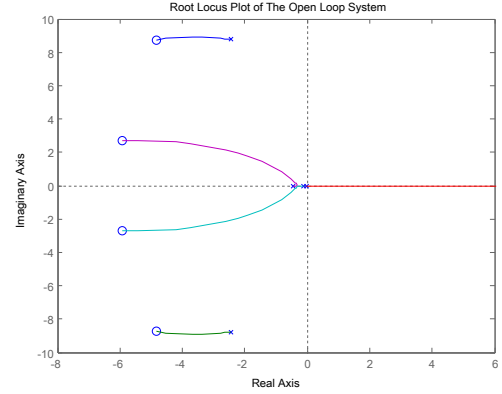


Fig. 7 Root locus of the open loop altitude dynamics of our flying-wing airframe

Meanwhile, Fig 7 depicts the root locus of the open loop transfer function of elevon average-to-altitude. It is apparent that there are two poles located near the origin that can cause instability for the overall open loop system. Fig 7 also clearly illustrates the coordinate position of the position of subsidence dominant poles with respect to short-term counterparts.

III. Uncertainty and Robustness

This section explicates the framework of our robust flight control system to the longitudinal flight motion of the Unmanned Aerial Vehicles, P15035. While we mainly focus on design based on μ -synthesis approach, we will also briefly compare the performance of our μ -synthesis closed-loop system with respect to H_∞ counterpart.

3.1 General Problem Formulations of Robust Autopilot

We bring our system into its equivalent MIMO model formulation. The plant in Fig. 9 can be represented in the following extended state space diagram as follows:

$$\begin{aligned} \dot{\tilde{x}} &= A\tilde{x} + B_1w + B_2u, \\ z &= C_1\tilde{x} + D_{11}w + D_{12}u, \\ y &= C_2\tilde{x} + D_{21}w + D_{22}u, \end{aligned} \quad (9)$$

where z is the regulated outputs, that is, the signal we are interested in controlling (in this research: altitude and its control signal), meanwhile, y

is signals that are measured and fed back to the controller. Also, w, u, x correspond to the existing disturbances, input elevon average, and states of the system, respectively.

The model of the system and the existing disturbance can be represented in the collapse block diagram shown in Fig. 8.

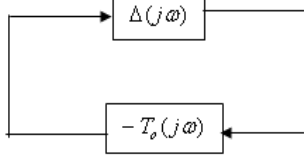


Fig. 8 Robust Stability Represented in Collapse Block Diagram

For stability analysis, the command reference signal is not required; hence it is set to be zero. Let $\Delta(j\omega)$ be the maximum uncertainty that can be tolerated by the closed loop control system while still maintaining its stability, and $T_o(j\omega) = L_o / (1 + L_o)$ be the complementary sensitivity function in which L_o is the open loop gain.

According to the small gain theorem, the stability of closed loop system can be guaranteed if $\|\Delta(j\omega)T_o(j\omega)\|_\infty < 1$. In other words, it can also be mathematically rewritten as:

$$|\Delta(j\omega)| < \frac{1}{|T_o(j\omega)|}, \quad \forall \omega \quad (11)$$

3.2 The Framework of our μ -synthesis Robust Autopilot

The control objective we would like to achieve is to synthesise a stabilizing μ -synthesis autopilot that can achieve the closed-loop performance objectives e.g. the desired (minimum) sensitivity function below 0 db over a particular frequency range.

The block diagram of our μ -synthesis robust autopilot can be depicted in Fig 9.

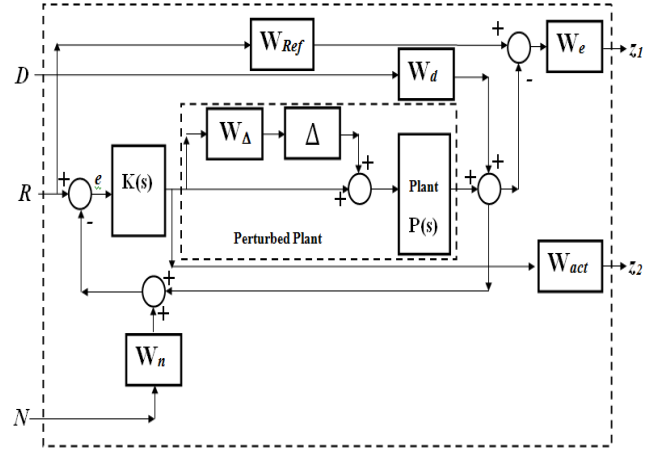


Fig. 9 μ -synthesis robust autopilot for altitude dynamics of a flying wing aircraft $z = T(P, K)w$, $z = [z_1 \ z_2]^T$, $w = [DR \ N]^T$.

To properly design our μ -synthesis robust-autopilot, we proceed as follows (as illustrated in Fig 9). First, the plant is modelled in the form of nominal model $P(s)$ and the multiplicative uncertainty model $W_\Delta \Delta$. $\|\Delta\|_\infty \leq 1$ denotes the complex structured uncertainty dynamics and the weighting function W_Δ shall determine the uncertainty as a function of frequency.

This model will be implemented to accommodate the error as an uncertainty model with respect to the input. We choose Δ in the form of a stable first-order transfer function.

Second, we define reference model W_{ref} which represents the desired model for the closed loop control system. We also define W_d and W_n which indicate the frequency characteristics of the external disturbance and the frequency domain noise in the feedback signals. This model will be derived based on the wind disturbance as depicted in [21].

Subsequently, we define W_e as the weighting function of the performance of the closed loop system with respect to our ideal response, while W_{act} is to shape the penalty control signal due to the limitation of the actuator at high frequency [20].

Given the framework of our control system in Fig. 10, the input vector of the weighted closed-loop

control systems is given by: $w = [D, R, N]^T$ while

the output vector can be denoted by $z = [z_1 \ z_2]^T$. Given the transfer function $T(P, K)$ as the closed-loop MIMO system, we can rewrite it as $z = T(P, K)w$.

Considering Fig. 10, we aim to work out the stabilizing autopilot $K(s)$ such that for all perturbations, the closed loop system $T(s)$ is stable, that is, to achieve $\|T[(P, \Delta_p), K]\|_\infty \leq 1$. In other words, the goal of μ -synthesis is to work out the stabilizing controller K so that $\min_K \max_\omega \{\mu_{\Delta_p}[T(s)]\}$ can be satisfied.

This can be performed by minimising the singular value $\mu_{\Delta_p}(\cdot)$ of the closed loop transfer function, where $\Delta_p \in \mathcal{A}$ is defined as hypothetical uncertainty block with respect to robust performance and \mathcal{A} denotes the augmented block structure

mathematically defined as: $\mathcal{A} = \begin{Bmatrix} \Delta & 0 \\ 0 & \Delta_p \end{Bmatrix}$. In addition, while $P(s)$ denotes open loop model of the system $K(s)$ indicates the robust compensator designed.

The μ -synthesis algorithm works by adopting the generalized scaled plant model $P(s)$ given by equation (10). The D - K iteration procedure is an approximation to μ -synthesis control design. It involves a sequence of minimisations, first over the controller variable K (holding the D variable associated with the scaled μ upper bound fixed), and then over the D variable (holding the controller K variable fixed). Interested readers may refer to [1] as well as [6, 7].

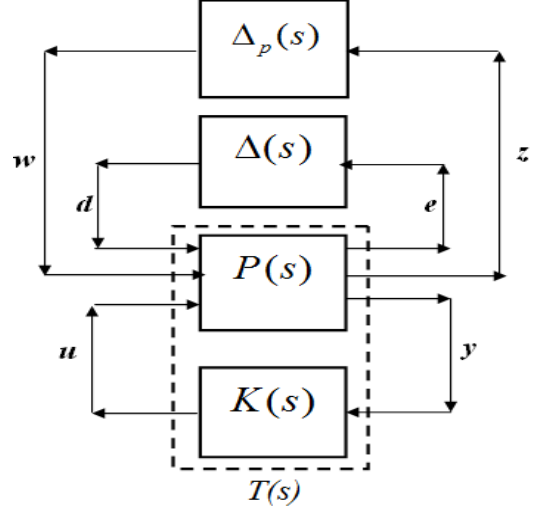


Fig. 10 μ -synthesis problem formulation in two port block diagram

The μ calculation (from the previous step) provides frequency-dependent scaling matrices D_f . The fitting procedure fits these scaling with rational, stable transfer function matrices.

$$\bar{\sigma}(D_f(j\omega)F_L(P, K)(j\omega)D_f^{-1}(j\omega))$$

$$\bar{\sigma}(\hat{D}_f(j\omega)F_L(P, K)(j\omega)\hat{D}_f^{-1}(j\omega))$$

The rational is absorbed into the open-loop interconnection for the next controller synthesis. Using either the previous frequency-dependent D 's or the just-fit rational, an estimate of an appropriate value for the H-norm is made. This is a conservative value of the scaled closed-loop H norm, using the most recent controller and either a frequency sweep (using the frequency-dependent D 's) or a state-space calculation (with the rational D 's).

IV. Design of μ -synthesis Robust Autopilot

To model the dynamic of the plant, we will be using extended state space equation as a direct conversion from the transfer function discussed in Section II. We can rewrite the open loop model as follows:

$$\begin{aligned} \dot{x}_1 &= -5.4740x_1 - 86.05x_2 - 49.12x_3 - 4.927x_4 - 0.065x_5 + u + d_1, \\ \dot{x}_2 &= x_1, \\ \dot{x}_3 &= x_2, \end{aligned} \quad (13)$$

$$\begin{aligned}\dot{x}_4 &= x_3, \\ \dot{x}_5 &= x_4 + d_3,\end{aligned}$$

Furthermore, the measurement equation is given by:

$$y = -0.0117x_1 - 0.2519x_2 - 3.006x_3 - 18.64x_4 - 49.42x_5 + n + d_2 + d_4,$$

where n is the existing noise in measurements.

The regulated outputs are altitude x_5 and control signal u , given as:

$$z = \begin{bmatrix} x_5 \\ u \end{bmatrix}, \quad (14)$$

in which z is the regulated output. In this design, the magnitude of control signal is to be bounded in the regulated outputs to avoid saturation issues. This requirement is also to satisfy the rank condition.

We will define the uncertain nature of our mathematical model as follows. At low frequency, below 2 rad/s, it can vary up to 25% from its nominal value. Around 2 rad/s the percentage variation starts to increase and reaches 400% at approximately 32 rad/s. The percentage model uncertainty is represented by the weight

$$W_\Delta = \frac{4.8(s+2)}{(s+32)} \quad \text{which corresponds to the frequency variation of the model uncertainty and the uncertain LTI dynamic object.}$$

Furthermore, a weighted sensitivity minimization

problem selects a weight $W_p = \frac{0.25s+0.6}{s+0.006}$, which corresponds to the inverse of the desired sensitivity function of the closed-loop system as a function of frequency. Hence the product of the sensitivity weight W_p and actual closed-loop sensitivity function is less than 1 across all frequencies. The sensitivity weight W_p has a gain of 100 at low frequency, begins to decrease at 0.006 rad/s, and reaches a minimum magnitude of 0.25 after 2.4 rad/s.

Subsequently, we employ second order model to represent the desired transfer function for the closed-loop control systems to achieve critically damped

$$W_{ref} = \frac{\omega_n^2}{s^2 + \xi\omega_n s + \omega_n^2}, \xi = 1, \omega_n = 1.5\pi$$

response:

In addition, we employ the model given in [21] to represent strong wing disturbance given by the following first order system:

$$W_d = \frac{15}{s+0.15}$$

Meanwhile for process and measurement noise, we consider the following first order model:

$$W_n = 10^{-5} \frac{s+10}{s+100}$$

Furthermore, we also weigh the performance of the closed-loop system compared to the ideal response. We follow the recommendation in [21], that suggests

W_e is flat at low frequency then rolls off at first order and flattens out at a small non-zero value at high-frequency, that is,

$$W_e = 200 \frac{s+1}{s+200}$$

Likewise, we also use the same model to shape the penalty of the control signal usage to limit input magnitudes at high frequency.

The resulting closed-loop eigen-values, damping factor as well as undamped natural frequency are given in Table 2.

Table 2 The resulting closed-loop pole's positions for μ -synthesis autopilot

Eigenvalue	Damping	Freq. (rad/s)
-6.00e-003	1.00e+000	6.00e-003
-5.84e-003+1.65e-003i	9.62e-001	6.07e-003
-5.84e-003-1.65e-003i	9.62e-001	6.07e-003
-1.55e-002	1.00e+000	1.55e-002
-1.55e-002	1.00e+000	1.55e-002
-1.55e-002	1.00e+000	1.55e-002
-1.58e-002	1.00e+000	1.58e-002
-1.09e-001	1.00e+000	1.09e-001
-1.09e-001	1.00e+000	1.09e-001
-1.09e-001	1.00e+000	1.09e-001
-1.09e-001	1.00e+000	1.09e-001
-1.09e-001	1.00e+000	1.09e-001
-2.72e+000	1.00e+000	2.72e+000
-4.90e+000	1.00e+000	4.90e+000
-5.93e+000+2.63e+000i	9.14e-001	6.49e+000
-5.93e+000-2.63e+000i	9.14e-001	6.49e+000
-4.84e+000+8.73e+000i	4.85e-001	9.98e+000
-4.84e+000-8.73e+000i	4.85e-001	9.98e+000
-3.93e+003	1.00e+000	3.93e+003

The resulting μ -synthesis autopilots is given in the following equation: (15)

$$K(s) = \frac{138724(s+32)(s+0.4632)(s+0.1087)(s+0.01553)(s+0.005996)(s^2+4.887s+83.12)}{(s+3927)(s+7.248)(s^2+0.01168s+0.00003682)(s^2+11.83s+42)(s^2+9.679s+99.72)}$$

Design of μ -synthesis autopilot has been successfully performed via D-K iteration. The D-K iteration procedure is an approximation to μ -synthesis control design. The objective of μ -synthesis is to minimise the structure singular value μ of the corresponding robust performance problem associated with the uncertain system $P(s)$.

The uncertain system $P(s)$ is given by the open-loop interconnection containing known components including the nominal plant model, uncertain parameters (μ -complex) and unmodeled LTI dynamics and performance and uncertainty weighting functions.

IV.1 H_∞ mixed-sensitivity loop shaping

Furthermore, as a benchmark performance, we will compare the performance of our μ -synthesis autopilot with respect to well-known H_∞ mixed-sensitivity autopilots as given in Fig 11 as follows.

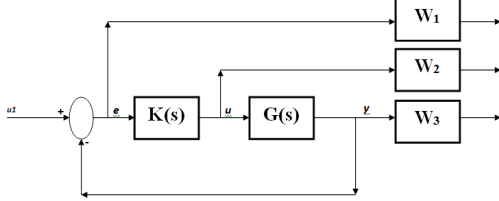


Fig. 11 The Framework of our H_∞ mixed-sensitivity autopilot

$$W_1 = 2 \frac{s+100}{10s+1}$$

We define $W_1 = 2 \frac{s+100}{10s+1}$ to weigh the error signal of our closed loop control system, while we weigh our actuator signal by a constant $W_2 = 0.1$ and the output signal is by a unity factor.

The resulting H_∞ compensator is given as follows:

$$K(s) = \frac{-392012.618(s+0.4632)(s+0.1087)(s+0.01553)(s^2+4.887s+83.12)}{(s+5641)(s+0.1)(s^2+6.788s+15.1)(s^2+5.342s+81.9)}$$

Accordingly, the corresponding eigen values of the closed loop control systems are given in Table 2.

Table 2 The resulting closed-loop pole's positions for H_∞ autopilot

Eigen-values	Damping	Frequency (rad/s)
-3.36e+000	1.00e+000	3.36e+000
-2.37e+000+ 2.67e+000i	6.64e-001	3.57e+000
-2.37e+000 - 2.67e+000i	6.64e-001	3.57e+000
-2.47e+000+ 8.79e+000i	2.71e-001	9.13e+000
-2.47e+000 - 8.79e+000i	2.71e-001	9.13e+000
-5.64e+003	1.00e+000	5.64e+003

-3.36e+000	1.00e+000	3.36e+000
-2.37e+000+ 2.67e+000i	6.64e-001	3.57e+000
-2.37e+000 - 2.67e+000i	6.64e-001	3.57e+000
-2.47e+000+ 8.79e+000i	2.71e-001	9.13e+000
-2.47e+000 - 8.79e+000i	2.71e-001	9.13e+000
-5.64e+003	1.00e+000	5.64e+003

4.1 Frequency Response

Classical stability margin can be represented using two parameters *i.e.* gain margin (GM) and phase margin (PM). Gain margin is defined as the factor by which the gain can be increased before the system is unstable. It also becomes the standard measure of the system's relative stability. The gain margin of a stable system has to be positive. This is also desirable from the point of view of robustness. Another parameter associated with relative stability is called phase margin, which indicates the additional phase lag that will make the system marginally stable.

The resulting Bode diagram and Nyquist plot of the compensated open loop transfer function is given by Fig. 12 and Fig 13 respectively.

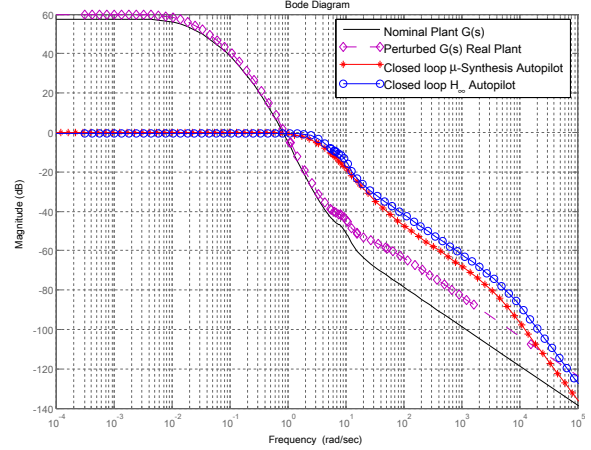


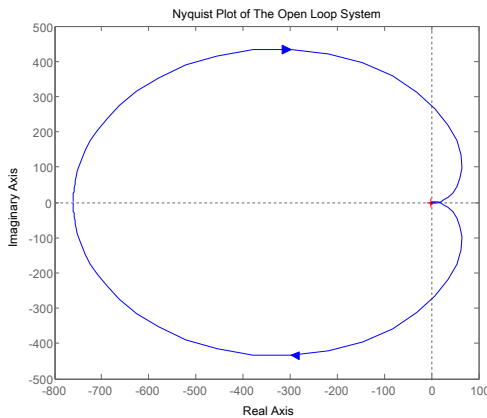
Fig. 12 Comparative Frequency Responses

The frequency response of the open loop system is given by solid black line while its perturbed modes is indicated by purple diamond line. The error in modelling is more noticeable at higher frequency, particularly for any ω greater than 10 rad/s as seen in Fig. 12.

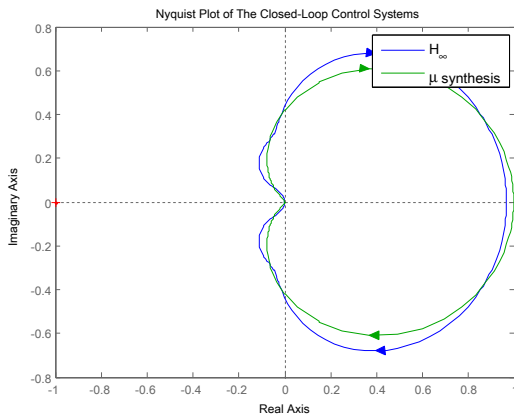
The closed loop control systems (both μ -synthesis and H_∞ autopilot) have successfully stabilised and

improved the performance of the system by satisfying the small gain theory so that $\|T[(P, \Delta_p), K]\|_{\infty} \leq 1$ can be satisfied for all frequency range. Furthermore, they also have significantly increased the bandwidth of the closed loop system with respect to open loop counterparts by a factor of two. In other words, the closed loop control systems have satisfied small gain theorem $\|\Delta(j\omega)T_o(j\omega)\|_{\infty} < 1$ leading to good stability margin and improved bandwidth by a factor of two.

Likewise, according to Nyquist plot in Fig. 13a, it is apparent that while the Nyquist plot of the open loop system encircles $-1+j0$, which indicates an unstable system, the Nyquist plot of the closed loop control systems, by no means, encircles the critical point $-1+j0$ since they have already satisfied the small gain theorem $\|T[(P, \Delta_p), K]\|_{\infty} \leq 1$.



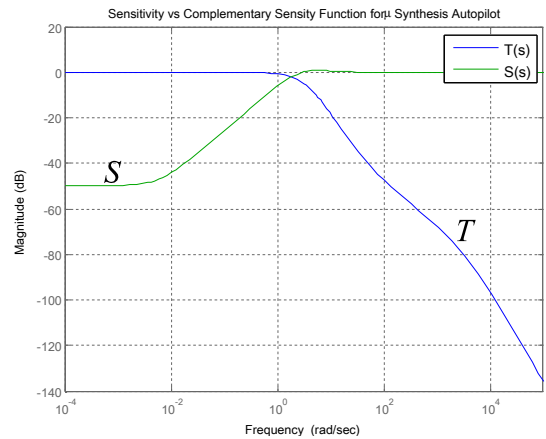
(a) Nyquist Plot of the Open Loop Transfer Function



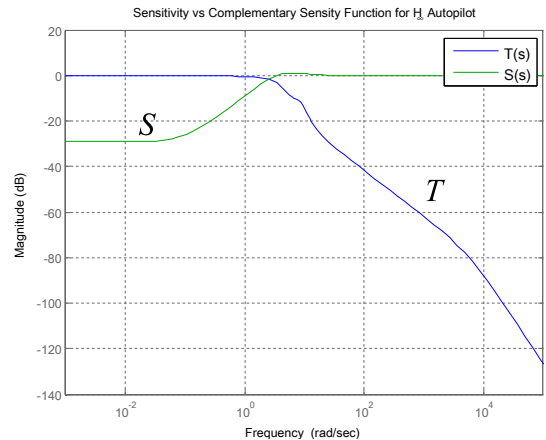
(b) Nyquist Plot of the Closed Loop Control Systems indicating $\|T[(P, \Delta_p), K]\|_{\infty} \leq 1$

Fig. 13 Comparative Nyquist Plots for Uncompensated and Compensated Systems

The resulting sensitivity vs. complementary sensitivity function for our μ -synthesis system is plotted in Fig. 14. It clearly depicts the *water bed* effect of our μ -synthesis system. It is also apparent that for $|L_o| \ll 1$, $|L_o| \approx |T_o|$, meanwhile for $|L_o| \gg 1$, $L_o \approx 1/S_o$. Thus, we can expect our system to possess low sensitivity at low frequency and low transfer function at higher-frequency. In other words, this turns out that at low frequency our system is expected to achieve better performance, while at high frequency it is anticipated to accommodate better robust stability margin.



(a) μ -synthesis autopilot



(b) H_{∞} autopilot

Fig. 14 Sensitivity vs. Complementary Sensitivity Function

4.2 Time Domain Performances

The feasibility of our μ -synthesis autopilot is now investigated in time domain as given by Fig. 15.

Given the configuration of the closed-loop control systems' poles, we have successfully achieved smooth and autonomous taking-off and landing systems with minimum overshoot and with reasonably short settling-time. However, while our μ -synthesis autopilot has slightly longer settling time compared to our H_∞ counterpart, it can achieve smoother response as proven by the absence of overshoot.

Overshoots are undesirable transient responses which have to be suppressed. Failure to accomplish this task may create some damages and lead to the failure of the system, particularly when the pilot would like to land the aircraft. It is also a waste of energy during taking off and landing process.

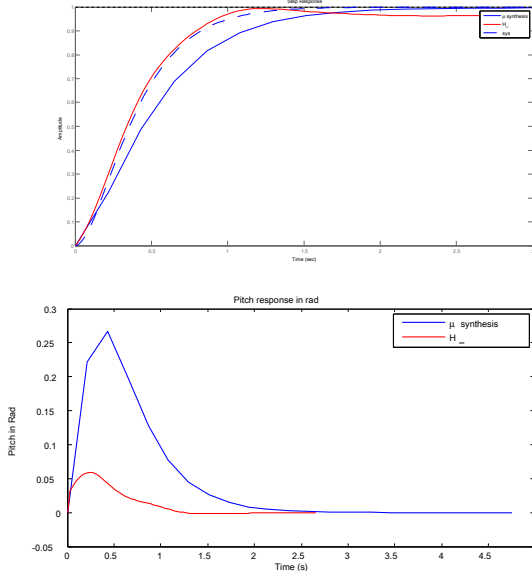


Fig. 15 Time domain performance of the closed loop control systems (taking off, cruising and landing) for altitude and pitch

4.3 Maximum Tolerable Amount of Uncertainty $\Delta(j\omega)$

At any given frequency, say for instance, ω_1 , the maximum amount of uncertainty $\Delta(j\omega)$ that can

be tolerated while still maintain the stability of the closed loop control system is the reciprocal of the amplitude of the complementary sensitivity function, $\|1/T_o(j\omega)\|$, as depicted by Fig 16.

It is clearly evident that within our system bandwidth our μ -synthesis autopilot has successfully outperformed H_∞ compensator in accommodating more uncertainty. This will clearly be beneficial for designing a real-time controller that can give better stability robustness to minimise the adverse impact of uncertainties (e.g. modelling error, noise, etc).

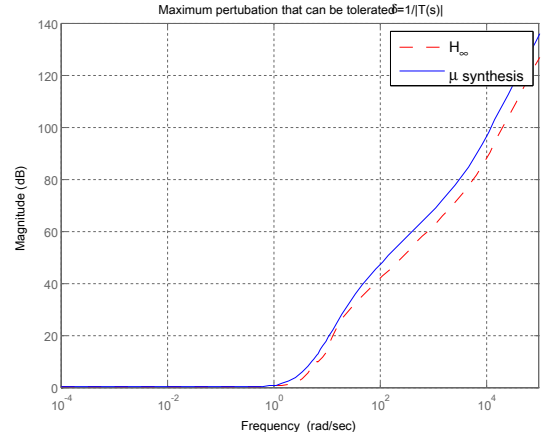


Fig. 16 Maximum Tolerable Amount of Uncertainty, $\Delta = 1/|T(j\omega)|$ for μ -Synthesis Autopilot as denoted by blue line H_∞ denoted by dotted green line.

V. Conclusion and Future Work

This paper presents a comparative study of powerful robust autopilots: μ -synthesis algorithm via D-K iteration with respect to conventional H_∞ counterpart. It has been clearly demonstrated that the proposed closed-loop control systems have successfully achieved reasonably short time domain response in the absence of overshoot and also achieved substantially good stability margin ($GM = \infty$ and $PM > 0$).

Compared to conventional H_∞ autopilot, our new μ -synthesis autopilot can accommodate more uncertainty as illustrated by several db improvement in the value of $\Delta(j\omega)$ for both lower and higher frequency e.g. starting from $\omega \geq 1$ rad/s.

This is essential since this frequency range is within the bandwidth of the closed loop control systems. Therefore, the proposed control schemes have clearly given better robust stability margin in terms of maximum tolerable amount of uncertainty that can be accommodated within their operational bandwidths.

Lastly, the time domain response of our μ -synthesis autopilot has also achieved more desirable response due to the absence of overshoot which is indeed not only safer but also more efficient for the operational of the aircraft itself.

Beyond linear modelling and robust control, in our future work, we shall consider non-linear modelling and autopilot for several reasons [36]. The first reason is due to the maturity of non-linear control, as with linear-control, supported with a variety of powerful methods and a successful history of industrial applications. The second reason is due to its intuitiveness and possibility to make it simple since the design process of non-linear controls are often deeply rooted from the physics of the plants.

Acknowledgements

The authors wish to thank Mr. Raymond Cooper, **our** Chief Test Pilot for his coordination of all test flights and the construction of the P15035 aircraft. We also wish to thank the **then** members of the **then** Aerobotics® Research Group at Monash University. Fendy Santoso was supported by an Australian Government Scholarship. The authors gratefully acknowledge the contribution from anonymous referees whose efforts greatly improved the presentation of this manuscript.

List of References

[1] H. Chao, Y. Cao and Y. Chen “Autopilots for small unmanned aerial vehicles: A Survey”, *International Journal of Control, Automation and Systems* February 2010, Volume 8, Issue 1, pp 36-44.

[2] A. R. Shabayek, C. Demonceaux, O. Morel, D. Fofi, “Vision Based UAV Attitude Estimation: Progress and Insights” , *Journal of Intelligent & Robotic Systems*, January 2012, Volume 65, Issue 1-4, pp 295-308.

[3] F. Santoso “Sub-optimal decentralised control algorithms for blanket and k-barrier coverage in autonomous robotic wireless sensor networks” *IET Communications*, vol.4, no.17, pp. 2041-2057, Nov. 26, 2010.

[4] M. Goodrich, B. S. Morse, D. Gerhardt, J. L. Cooper, M. Quigley, J. A. Adams, C. Humphrey, “Supporting wilderness search and rescue using a camera-equipped mini UAV”, *Journal of Field Robotics*, Special Issue: Special Issue on Search and Rescue Robots, Volume 25, Issue 1-2, pages 89–110, January - February 2008.

[5] F. Santoso “A Decentralised Self-Dispatch Algorithm for Square-Grid Blanket Coverage Intrusion Detection Systems in Wireless Sensor Networks”, *IEEE Vehicular Technology Conference (VTC Fall)*, 2011, vol. 1, no. 5, pp. 5-8 Sept. 2011.

[6] G. J. Balas, A.K. Packard and J.T. Harduvel 1991, “Application of μ -synthesis techniques to momentum management and attitude control of the space station” *AIAA Guidance, Navigation and Control Conference*, New Orleans, August.

[7] G. J. Balas, and J. C. Doyle March-April, 1994, “Robust control of flexible modes in the controller crossover region”, *AIAA Journal of Guidance, Dynamics and Control*, Vol. 17, no. 2, pp. 370-377.

[8] J. C. Doyle, P. Glover, and Francis, B. August 1989, “State-space solutions to standard H_2 and H_∞ control problems”, *IEEE Transactions on Automatic Control*, vol. 34, no. 8, pp. 831-847,.

[9] J. C. Doyle, B. Francis, and A. Tannenbau, 1990, “Feedback Control Theory”, Mac Milan Publishing Co.

[10] A. Packard, J. Doyle, and G. Balas, *Linear*, “Multivariable Robust Control with a μ perspective”, *ASME Journal of Dynamic Systems, Measurement and Control*, 50th Anniversary Issue, vol. 115, no. 2b, pp. 310-319, June 1993.

[11] J. C. Doyle, K. Lenz, and A. Packard 1987, “Design examples using μ -synthesis: Space shuttle lateral axis FCS during re-entry”, *NATO ASI Series, Modelling, Robustness, and Sensitivity Reduction in Control Systems*, vol. 34, Springer-Verlag.

[12] K. Glover and J. C. Doyle, “State-space formulae for all stabilizing controllers that satisfy an H norm bound and relations to risk

- sensitivity”, *Systems and Control Letters*, 1988. vol. 11, pp. 167-172.
- [13] K. Zhou and J. Doyle, “Essentials of Robust Control”, Prentice Hall.
- [14] G. Stein, and J. Doyle, “Beyond singular values and loop shapes”, *AIAA Journal of Guidance and Control*, vol. 14, num. 1, pp. 5-16, 1991.
- [15] M.G. Safonov, A. J. Laub, and G. Hartmann, “Feedback Properties of Multivariable Systems: The Role and Use of Return Difference Matrix”, *IEEE Trans. of Automat. Control*, AC-26, pp. 47-65.
- [16] B. Kulcsar, , “LQG/LTR Controller Design for an Aircraft Model”, *Periodica Polytechnica Ser*, Vol. 28, No. 1-2, PP 131-142.
- [17] L. B. Stevens and F. Lewis, “Aircraft Control and Simulation”, John Wiley & Sons, Inc, 2nd edition, 2003.
- [18] R. Pratt, “Flight Control Systems: Practical Issues in Design and Implementation”, The Institution of Electrical Engineers, UK, 2000.
- [19] A. J. R. Bryson, “Control of Spacecraft and Aircraft”, Princeton University Press, NJ.
- [20] P. Melin and O. Castillo, “A New Neuro-Fuzzy-Fractal Approach for Adaptive Model-Based Control of Non-Linear Dynamic Systems: The Case of Controlling Aircraft Dynamics”, *IEEE International Fuzzy Systems Conference Proceedings*, August 22-29, 1999, Seoul, Korea
- [21] Z. Ye, P. Bhattacharya, H. Mohamadian, H. Majleseini, Y. Ye, “Equational Dynamic Modeling and Adaptive Control of UAV”, *Proceedings of the 2006 IEEE/SMC International Conference on System of Systems Engineering*, Los Angeles, CA, USA - April 2006
- [22] J. Escareño, S. Salazar and R. Lozano, “Modelling and Control of a Convertible VTOL Aircraft”, *Proceedings of the 45th IEEE Conference on Decision & Control Manchester Grand Hyatt Hotel, San Diego, CA, USA, December 13-15, 2006*
- [23] B. P. Rimal, H. Shin and E. Choi, “Simulation of Nonlinear Identification and Control of Unmanned Aerial Vehicle: An Artificial Neural Network Approach”, *9th International Symposium on Communications and Information Technology, (ISCIT-2009)* pp.442,447, 28-30 Sept. 2009
- [24] V.I.George, Joyson D’Souza, Ciji Pearl Kurian, I.Thirunavukkaras “A Simulink Model for an Aircraft Landing System Using Energy Functions”, *7th IEEE Conference on Industrial Electronics and Applications (ICIEA), 2012*, pp. 355-360, 18-20 July 2012.
- [25] W. Yuan, J. Katupitiya “Design of a μ -Synthesis Controller to Stabilise an Unmanned Helicopter”, *28th International Congress of The Aeronautical Sciences (ICAS-2012)*, 23rd - 28th September 2012, Brisbane, Australia.
- [26] B. Boulet, B. A. Francis, P. C. Hughes, T. Hong, “ μ -Synthesis for a Large Flexible Space Structure Experimental Testbed”, *Journal of Guidance, Control, and Dynamics*, Vol. 24, No. 5, September–October 2001, pp. 967-977.
- [27] M. Liu, G. Egan and Y. Ge, “Identification of Attitude Flight Dynamics for an Unconventional UAV”, *Proc. of IEEE/RSJ International Conference on Intelligent Robots and Systems*, Oct. 9-15, Beijing, China, 2006.
- [28] F. Santoso, M. Liu, and G. Egan, H_2 and H_∞ “Robust Autopilot Synthesis for longitudinal flight of a Special Unmanned Aerial Vehicle: A comparative Study”, *IET Control theory and Applications* Volume 2 Issue 7, pp. 583–594, 2008
- [29] F. Santoso, M. Liu and G. Egan, “Optimal Control Linear Quadratic Synthesis for an Unconventional Aircraft”, *Proc. of Twelfth Australian International Aerospace Congress (AIAC-12)*, Melbourne, 19-22 March 2007, *also as MECSE-5-2007*, Department of Electrical & Computer Systems Engineering, Monash University, 2006.
- [30] W. Juan and J. Katupitiya, “Design of a μ -synthesis autopilot to stabilise and unmanned helicopter”, *28th International Congress of the Aeronautical Sciences (ICAS2012)*.
- [31] Balas G. Chiang R, Packard A and Safonov M., “Robust Control Toolbox for Use with Matlab”, The Mathworks, Inc, 2006.
- [32] P. Eykhoff, “System Identification: Parameter and State Estimation”, John Wiley & Sons.
- [33] G. C Goodwin, and R. L. Payne, “Dynamic system identification: Experiment design and data analysis”, Academic Press, INC London, Ltd.

- [34] R. K. Mehra and D. G. Lainiotis, "System Identification Advances and Case Studies", Academic Press, INC. (London) Ltd.
- [35] Sage, A. P. and Melsa, J. L. 1971, "System Identification", Academic Press, INC, London, Ltd.
- [36] J.J. E. Slotine, W. Li. "Applied Non-Linear Control" Prentice Hall International, USA